Independent application of an analytical model for secondary neutron equivalent dose produced in a passive-scattering proton therapy treatment unit

Independent application of an analytical model for secondary neutron equivalent dose produced in a passive-scattering proton therapy treatment unit

Kyle J Gallagher[1,2] and Phillip J Taddei[3,4]
(1) Oregon Health and Science University, Portland, Oregon, (2) Oregon State University, Corvallis, Oregon, (3) American University of Beirut Medical Center, Beirut, Lebanon, (4) University of Washington School of Medicine, Seattle, Washington

Corresponding author address: Phillip Taddei, Department of Radiation Oncology, University of Washington School of Medicine, 1959 NE Pacific Street, Box 356043, Seattle, WA, 98195, USA. Tel.: +1-206-306-2835; Fax: +1-206-417-0347; Email: ptaddei@uw.edu

Revised manuscript: June 28, 2018

Abstract

Purpose: To independently apply an analytical model for equivalent dose from neutrons produced in a passive-scattering proton therapy treatment unit, *H*.

Methods: To accomplish this objective, we applied the previously-published model to treatment plans of two pediatric patients. Their model accounted for neutrons generated by mono-energetic proton beams stopping in a closed aperture. To implement their model to a clinical setting, we adjusted it to account for the area of a collimating aperture, energy modulation, air gap between the treatment unit and patient, and radiation weighting factor. We used the adjusted model to estimate *H* per prescribed proton absorbed dose, D_{Rx}, for the passive-scattering proton therapy beams of two children, a 9-year-old girl and 10-year-old boy, who each received intracranial boost fields as part of their treatment. In organs and tissues at risk for radiation-induced subsequent malignant neoplasms, *T*, we calculated the mass-averaged *H*, H_T, per D_{Rx}. Finally, we compared H_T/D_{Rx} values to those of previously-published Monte Carlo (MC) simulations of these patients' fields.

Results: H_T/D_{Rx} values of the adjusted model deviated from the MC result for each organ on average by 20.8 ± 10.0% and 44.2 ± 17.6% for the girl and boy, respectively. The adjusted model underestimated the MC result in all *T* of each patient, with the exception of the girl's bladder, for which the adjusted model overestimated H_T/D_{Rx} by 3.1%. The adjusted model provided a better estimate of H_T/D_{Rx} than the unadjusted model. That is, between the two models, the adjusted model reduced the deviation from the MC result by approximately 37.0% and 46.7% for the girl and boy, respectively.

Conclusion: We found that the previously-published analytical model, combined with adjustment factors to enhance its clinical applicability, predicted H_T/D_{Rx} in out-of-field organs and tissues at risk for subsequent malignant neoplasms with acceptable accuracy. This independent application demonstrated that the analytical model may be useful broadly for clinicians and researchers to calculate equivalent dose from neutrons produced externally to the patient in passive-scattering proton therapy.

1. Introduction

Nontherapeutic stray neutrons are produced in the delivery of proton therapy beams. These neutrons are of concern because of their high and uncertain relative biological effectiveness for late effects such as carcinogenesis (Grahn *et al* 1992, Wolf *et al* 2000, Hollander *et al* 2003, Kuhne *et al* 2009). Neutrons produced in the patient are unavoidable, but neutrons generated in the treatment unit, i.e., "external neutrons," may be attenuated by simple modifications to the treatment unit (Taddei *et al* 2008, Taddei *et al* 2009b, Brenner *et al* 2009). In passive-scattering proton therapy (PSPT), the final collimating aperture is the chief source of patient exposures to external neutrons (Pérez-Andújar *et al* 2009, Matsumoto *et al* 2016). Because commercial treatment planning systems in proton therapy do not calculate the equivalent dose from external neutrons, H, a vast number of research studies into H have applied detailed Monte Carlo (MC) simulations (Fontenot *et al* 2005, Jiang *et al* 2005, Polf and Newhauser 2005, Polf *et al* 2005, Tayama *et al* 2006, Zheng *et al* 2007a, Zheng *et al* 2007b, Zheng *et al* 2008, Fontenot *et al* 2008, Moyers *et al* 2008, Newhauser *et al* 2008, Zacharatou Jarlskog *et al* 2008, Athar and Paganetti 2009, Fontenot *et al* 2009, Newhauser *et al* 2009, Taddei *et al* 2009a, Hultqvist and Gudowska 2010, Taddei *et al* 2010, Rechner *et al* 2012, Pérez-Andújar *et al* 2013, De Smet *et al* 2014, Zhang *et al* 2013, Zhang *et al* 2014, Geng *et al* 2015, Taddei *et al* 2015, Matsumoto *et al* 2016, Homann *et al* 2016, De Smet *et al* 2017, Han *et al* 2017, Taddei *et al* 2017). However, MC simulations of this type are time consuming and, among other reasons, not currently used in a clinical setting. Analytical models, on the other hand, may offer faster computations of H with acceptable accuracy (Newhauser *et al* 2017).

One such model has been developed by Newhauser and co-workers over the past decade and is nonproprietary and straightforward to implement. Basic versions were developed between 2006 and 2010 at The University of Texas MD Anderson Cancer Center (Zhang *et al* 2010) and advanced versions between 2011 and 2017 at Louisiana State University with collaborators from Mary Bird Perkins Cancer Center and other institutions (Pérez-Andújar *et al* 2013, Farah *et al* 2015, Schneider *et al* 2015, Eley *et al* 2015). For brevity, we shall refer to this model as the LSU-MDA model. The model estimates H per prescribed proton absorbed dose, D_{Rx}, in a water phantom. The version reported by Schneider *et al* (2015) was simpler to configure and use than previous versions and offered continuous applicability from 100 to 250 MeV in proton beam energy. Eley *et al* (2015) integrated the model into a proton therapy treatment planning system and extended the model to include range modulation and arbitrary collimator shapes. However, all of these studies were performed by the team who developed the LSU-MDA model, and, to date, an independent application had not been performed in a clinically relevant case.

The purpose of this study was to independently apply and evaluate the LSU-MDA model for H in PSPT in clinically realistic circumstances. Using the model, we estimated the average H in organs and tissues, T, at risk for subsequent malignant neoplasms (SMNs), H_T, for two children who received PSPT to an intracranial target. To do so, we adjusted the LSU-MDA model to account for the patients' treatment field parameters, namely, aperture size, range modulation, air gap, and radiation weighting factor, w_R. As a figure of merit for evaluation, we compared our estimated H_T values to those calculated by previously-published MC simulations.

2. Methods

2.1. Patient selection

Because MC simulations had already been performed, the boost treatment fields of the 10-year-old boy of Taddei *et al* (2009) and the 9-year-old girl of Taddei *et al* (2010) were selected for this study. In each study, MC calculations were performed using the Monte Carlo N-Particle eXtended code version 2.6b (Pelowitz 2008) to estimate the absorbed dose from external neutrons in each voxel, D_v, of the patients' simulated bodies. They applied the recommendations of the International Commission on Radiological Protection (ICRP) in Publication 92 (2003) to estimate the radiation weighting factor, w_R. With these parameters, they determined H in each voxel, v, as:

$$H_v = w_R \cdot D_v. \quad (1)$$

Each patient's plan included intracranial boost fields. These fields were similar in design to those of treatments for localized brain tumors, such as astrocytomas, ependymomas, and gliomas. Determining and minimizing out-of-field H for pediatric patients with brain tumors such as these is critical because they may have good long-term prognoses and are therefore at risk of developing late-effects of which SMNs are the chief concern (Armstrong *et al* 2010).

2.2. Patient diagnosis, prescription, and treatment planning

In the previous studies, treatment plans for a girl and a boy diagnosed with primitive neuroectodermal tumors were considered. Their treatments included intracranial boosts prescribed to deliver 21.3 Gy in the clinical target volume using PSPT. For the girl, the intracranial boosts comprised three fields of nominal energies (i.e., energies prior to beam shaping) at either 160 MeV or 180 MeV. The boy's two PSPT intracranial boost fields were of slightly lower nominal energies of 140 MeV and 160 MeV. The beam characteristics of the intracranial boost fields for these two children are summarized in Table 1. Further details of the computed tomography simulations, treatment plans, and MC techniques used for dose calculation can be found in the previous publications.

2.3. Translation of the analytical model to a clinical setting

The LSU-MDA analytical model for H considered four different external neutron energy regimes, contained 22 fitting parameters, and was continuous with proton beam energy from 100 to 250 MeV. We adjusted the model for translation to a clinical setting, accounting for w_R, spread-out Bragg peak (SOBP), aperture size, and air gap (the LSU-MDA model accounted for distance from the virtual neutron source but not for varying air gaps). We applied correction factors for each of these based on previous publications of generalized, detailed characterizations of the same PSPT treatment unit (Zheng *et al* 2007b, 2008). The equation for our adjusted model was the following:

$$H_v/D_{Rx} = F_{wR} \cdot F_{SOBP} \cdot F_{as} \cdot F_g \cdot H_{LSU-MDA,v}/D_{Rx}, \quad (1)$$

where F_{wR}, F_{SOBP}, F_{as}, and F_g were the adjustment factors for w_R, SOBP, aperture size, and air gap, respectively. $H_{LSU\text{-}MDA,v}/D_{Rx}$ was the H_v/D_{Rx} values as calculated by the LSU-MDA model.

The w_R used to determine H by the LSU-MDA model was considerably lower (approximately a factor of 1.7) than the w_R used in the previous MC datasets of the boy and girl, so we adjusted the w_R values to make a better comparison between the results of the analytical model and those of the MC simulations. We calculated F_{wR} in each voxel as the ratio of the MC studies' w_R value to the value

applied by the LSU-MDA model. The w_R values were not given by Schneider *et al*, so we approximated their values in each voxel by using equation 5 from their previous study (Pérez-Andújar *et al* 2013). This equation 5 calculated w_R as a function of depth and off-axis distance. In the MC studies, w_R was determined at isocenter for various proton beam energies based on ICRP Publication 92 (2003) (Figure 5a of Zheng *et al* [2008]). The w_R for the respective proton beam energies of the intracranial boost fields were used to calculate F_{wR}.

An SOBP adjustment factor was created to account for the lack of modulation in the analytical model. F_{SOBP} values were taken directly from Zheng *et al* (2008). In these studies, Zheng *et al* performed MC simulations comparing the neutron ambient dose equivalent per therapeutic proton absorbed dose at isocenter, $H^*(10)/D_{iso}$, from a nominal 250-MeV proton beam of various SOBP widths normalized to a pristine Bragg peak. We used the resulting values in their Figure 9a. The factor reflecting the relative increase in $H^*(10)/D_{iso}$ of the medium snout size for the respective SOBP width was directly used for F_{SOBP} (Table 1) and applied to each intracranial boost field.

We adjusted the model for the varying size of the aperture in the clinical treatment fields in our study. We derived F_{as} based on the results of the previous MC studies. Similar to SOBP, Zheng *et al* performed MC simulations comparing $H^*(10)/D_{iso}$ for various aperture sizes and a closed-aperture in their Figure 8 (Zheng *et al* 2008). However, this Figure 8 was not normalized to a closed-aperture. Therefore, F_{as} was determined as the ratio of $H^*(10)/D_{iso}$ of the medium snout size of each aperture area to that of the medium snout size with a closed aperture (Table 1).

To account for air gap, g, F_g was derived from the previous MC studies. Zheng *et al* (2007) conducted MC simulations to study the effect of distance from the treatment snout on H per the therapeutic absorbed proton dose, D_p, for a 250 MeV proton beam with medium and large snout sizes (their Figure 7). In our study of pediatric intracranial fields, the air gap was calculated as the difference of the snout position (i.e., distal portion of the treatment unit) and the surface of the patient along the central axis. In order to match this definition of air gap, we calculated air gap from Zheng *et al*'s study as the difference in the snout position and the isocenter minus the upstream radius of the tally volume. F_g was calculated from Zheng *et al* as the ratio of H/D_p that equated to the air gap of the intracranial fields and H/D_p that equated to the air gap used by Schneider *et al* to train their model, i.e, 15 cm. Thus, air gaps larger than 15 cm, e.g., those of the girl's fields, would result in F_g values less than 1, and air gaps smaller than 15 cm, e.g., those of the boy's fields, would result in F_g values greater than 1. The air gap of the boy's fields was only 2 cm, which is very rare in clinical applications but was maintained in our study so that we could compare our results with those of the previous publications. Because 2 cm was less than the smallest air gap studied by Zheng *et al*, we extrapolated beyond the scope of their data using the following logarithmic function:

$$H_Z/D_p = -11.81 \ln g + 50.767, \quad (2)$$

where H_Z/D_p was H/D_p as plotted in their Figure 7 and g was the corresponding air gap (cm). To verify the fitted function, previous MC simulations estimating the neutron equivalent dose of the left posterior oblique (LPO) field of the girl were compared to the similar LPO field of the boy. The main difference between the two fields was the air gap–23 cm for the girl's field and 2 cm for the boy's field. The neutron equivalent dose decreased by a factor of 2.7 when increasing the air gap from 2 cm to 23 cm,

which was consistent with the prediction of the above fitted function. Therefore, the fitted function was used to approximate the numerator of F_g for the boy.

H_T/D_{Rx} was determined for each component of the adjusted model and for all adjustments. First, we implemented the LSU-MDA model with the adjustment factors using in-house codes and commercial software (version R2014a, MATLAB, The MathWorks, Inc., Natick, Massachusetts) to calculate H_v/D_{Rx}. Second, we recycled the same contours for organs and tissues, T, from the previous publications for the girl and boy to compute mass-averaged H_T/D_{Rx}. We selected out-of-field T associated with site-specific SMN risk, including the esophagus, thyroid, heart, lungs, liver, small bowel, colon, stomach, kidneys, bladder, breast tissue, ovaries, testicles, and prostate. Finally, our values for H_T/D_{Rx} were compared to those of the previous MC studies of the girl and boy.

3. Results

3.1. Validation of the previous analytical model

The adjustment factors we found to account for SOBP, aperture area, air gap, and w_R of each intracranial beam are listed in Table 1. Only F_g differed considerably between the girl's fields and the boy's fields. F_g, the largest adjustment factor for the boy's fields, increased H_v/D_{Rx} by a factor of 2.22 for the boy's fields but decreased H_v/D_{Rx} by 36.3% for the girl's fields. The largest adjustment factors for the girl's fields were F_{SOBP} and F_{wR}. Unlike the other adjustment factors, F_{wR} varied for each voxel and therefore, the average F_{wR} was reported. The w_R for each field of the MC dataset of the girl and boy are also included in Table 1. Although the w_R approximated from Zheng *et al* are not explicitly shown in Table 1, these values of w_R were within 3% on average of the previous MC dataset of the girl and boy.

Figure 1 shows all H_T/D_{Rx} values from the girl's fields of the adjusted model compared to those of the previous MC studies. Before we applied any adjustment factors to the model, H_T/D_{Rx} calculated by the model was less than the MC results for all organs, on average by 57.4% ± 4.8%, i.e., approximately within a factor of 2. After applying all corrections, H_T/D_{Rx} calculated by the model was less than the MC results for all organs, on average by 20.8% ± 10.0%, with the exception of the bladder for which the model overestimated H_T/D_{Rx} by 3.0%. The maximum deviation of the model from the MC result was in the breast tissue, for which H_T/D_{Rx} calculated by the fully adjusted model underestimated the MC result by 39.0%.

Figure 2 shows all H_T/D_{Rx} values from the boy's fields of our adjusted model compared to those of the previous MC studies. Similar to the girl's fields, H_T/D_{Rx} of the unadjusted model was less than those of the MC for all organs. However, unlike the girl's fields, the unadjusted model grossly underestimated the MC results, on average by 91.4% ± 2.9%. After applying all adjustments, H_T/D_{Rx} calculated by the model underestimated the MC H_T/D_{Rx} by less than a factor of 2, at 44.2% ± 17.6% on average for all the organs. Unlike the girl's fields, the analytical model's dose estimation of the boy's fields diverged from the MC results with distance from the field edge. For example, H_T/D_{Rx} estimated in organs near the treatment field, i.e., esophagus, thyroid, heart, lungs, stomach, liver, and kidneys, were on average 31.7% ± 10.8% lower than the MC result whereas H_T/D_{Rx} estimated by the model in organs far from the treatment field, i.e., prostate, bladder, colon, rectum, and testicles, were 61.7% ± 5.1% on average lower than the MC result. The model's maximum deviation from the MC result was in the rectum, for which H_T/D_{Rx} estimated by the model underestimated that of the MC by 65.9%.

4. Discussion

In this study, we applied an analytical model for estimating equivalent dose from neutrons produced in a PSPT treatment unit and confirmed its ability to reproduce organ doses with accuracy similar to that of MC simulations for two pediatric patients with intracranial tumors. We performed this study independently of the team who developed the model. However, we made adjustments for clinical realism. Specifically, we attuned the model to account for SOBP, aperture area, air gap, and w_R.

Our aim was to test the feasibility of using a fast and simple analytical model to estimate external neutron equivalent dose with an acceptable level of accuracy but without the computational overhead and complexity of MC. After adjusting the model for clinical realism, we achieved this with similar accuracy to what was attained when validating MC results against measurements (Fontenot *et al* 2005, Wroe *et al* 2007, Howell and Burgett 2014). To estimate organ doses from external neutrons to within a factor of 2 using a simple analytical model is especially noteworthy considering the large uncertainties in w_R for neutrons, a radiological protection quantity that attempts to take into account the relative biological effectiveness of neutrons for carcinogenesis (Grahn *et al* 1992, Wolf *et al* 2000, Hollander *et al* 2003, Kuhne *et al* 2009). An adjusted analytical model gives clinicians the opportunity to routinely calculate equivalent dose from external neutrons for PSPT treatment units as well as researchers performing retrospective studies involving stray neutron equivalent dose, with the goal of lowering the risk of SMNs or other toxicities in survivors (Newhauser *et al* 2016, Berrington de González *et al* 2017, Stokkevåg *et al* 2017).

The impacts of adjusting the model differed between the two test cases. H_T/D_{Rx} of the unadjusted model adequately estimated the external neutron dose for the girl's fields (by a factor of 2-2.5) but underestimated the external neutron dose for the boy's fields (by a factor of 13). However, after our tested adjustments, H_T/D_{Rx} estimated by the model was generally within a factor of two of the MC result for both patients. One cause of the underestimation for the boy's was a very small 2-cm air gap between the treatment unit and the patient. A 2-cm air gap is rarely used in proton therapy and it was much smaller than the 15 cm air gap used to train the LSU-MDA model, and our F_g values for this small air gap were extrapolated far beyond the data of Zheng *et al*. The considerable deviation in the length of the air gap at treatment compared to the training data created an F_g of 2.22 for each of the boy's fields, deviating farther from 1 than F_g of the girl's fields, which were 0.64 ± 0.08 on average.

The H_T values after our adjustments to the LSU-MDA model, especially for the girl's fields, were even closer to the H_T values of the MC than those of Eley *et al* for a patient with Hodgkin's Lymphoma (2015). However, they accounted for different factors—range modulation, aperture area, and anatomical heterogeneities—than we did. For example, the application of the model by Eley *et al* reproduced H_{thyroid} to within 39% of the MC result while our application of the model estimated H_{thyroid} to within 13% and 34% of the MC for the girl and boy, respectively. In either case, within or independent of the LSU-MDA team, the model has been demonstrated in clinical cases to estimate H_T with accuracy comparable to that of MC or measurements (Agosteo et al 1998, Polf *et al* 2005, Farah *et al* 2014) and with greatly lessened computational overhead.

Our study had the following limitations. First, we applied the LSU-MDA model to two patients' treatments only. However, the realism of our work is notable. Second, we did not consider other reasonable adjustments to the model. For example, unlike Eley *et al*, we did not account for water equivalent thickness of heterogeneous tissue nor did we consider their nuclear cross sections.

Considering actual tissue compositions may affect neutron production by up to 40% (Moffitt *et al* 2018). Thus, accounting for tissue heterogeneities is another avenue for a potentially major improvement in the model. Another possible improvement over our adjustments may be to compensate for further complexities, such as the lateral dimensions of the proton beams incident on the aperture, the self-shielding of the aperture block, and integrating over a three-dimensional distribution of secondary neutron generation points in the aperture block rather than assuming a single point source. Although these omissions may have contributed to the general underestimation of H_T/D_{Rx} values from our adjusted model, we would expect their affects to be minor compared to the adjustments made in this study and in the study by Eley *et al*. Future developments of a more generalized analytical model may test and, if necessary, account for the effects of these and various other physical aspects of a modern clinical proton beam.

In conclusion, we independently applied and evaluated a fast and simple analytical model to estimate equivalent dose from neutrons generated in a PSPT treatment unit. We found its accuracy to be sufficient, for example, for the purpose of estimating the risks of radiogenic cancers. In particular, after applying clinically-relevant adjustment factors, the model provided satisfactory estimates of equivalent dose from external neutrons in out-of-field organs and tissues for two pediatric intracranial therapy treatment plans. This independent testing may be considered an avocation for further validation of analytical models for neutron doses in proton therapy, with the goal of understanding and minimizing neutron exposures and SMN risks.

Acknowledgements

Funding was in part by the Fogarty International Center (award K01TW008409), the Naef K. Basile Cancer Institute, and the Portland Chapter of the Achievement Rewards for College Scientists. The content is solely the responsibility of the authors and does not necessarily represent the official views of the sponsors.

References

Agosteo S, Birattari C, Caravaggio M, Silari M and Tosi G 1998 Secondary neutron and photon dose in proton therapy *Radiother Oncol* **48** 293–305

Armstrong G T, Stovall M and Robison L L 2010 Long-Term Effects of Radiation Exposure among Adult Survivors of Childhood Cancer: Results from the Childhood Cancer Survivor Study *Radiat Res* **174** 840–50

Athar B S and Paganetti H 2009 Neutron equivalent doses and associated lifetime cancer incidence risks for head & neck and spinal proton therapy *Phys Med Biol* **54** 4907–26

Berrington de González A, Vikram B, Buchsbaum J C, de Vathaire F, Dörr W, Hass-Kogan D, Langendijk J A, Mahajan A, Newhauser W, Ottolenghi A, Ronckers C, Schulte R, Walsh L, Yock T I and Kleinerman R A 2017 A Clarion Call for Large-Scale Collaborative Studies of Pediatric Proton Therapy *Int J Radiat Oncol Biol Phys* **98** 980–1

Brenner D J, Elliston C D, Hall E J and Paganetti H 2009 Reduction of the secondary neutron dose in passively scattered proton radiotherapy, using an optimized pre-collimator/collimator *Phys Med Biol* **54** 6065–78

De Smet V, De Saint-Hubert M, Dinar N, Manessi G P, Aza E, Cassell C, Vargas C S, Van Hoey O, Mathot G, Stichelbaut F, De Lentdecker G, Gerardy I, Silari M and Vanhavere F 2017 Secondary neutrons inside a proton therapy facility: MCNPX simulations compared to measurements performed with a Bonner Sphere Spectrometer and neutron H*(10) monitors *Radiat Meas* **99** 25–40

De Smet V, Stichelbaut F, Vanaudenhove T, Mathot G, De Lentdecker G, Dubus A, Pauly N and Gerardy I 2014 Neutron *H**(10) inside a proton therapy facility: Comparison between Monte Carlo simulations and WENDI-2 measurements *Radiat Prot Dosim* **161** 417–21

Eley J, Newhauser W, Homann K, Howell R, Schneider C, Durante M and Bert C 2015 Implementation of an Analytical Model for Leakage Neutron Equivalent Dose in a Proton Radiotherapy Planning System *Cancers* **7** 427–38

Farah J, Bonfrate A, De Marzi L, De Oliveira A, Delacroix S, Martinetti F, Trompier F and Clairand I 2015 Configuration and validation of an analytical model predicting secondary neutron radiation in proton therapy using Monte Carlo simulations and experimental measurements *Phys Medica* **31** 248–56

Farah J, Martinetti F, Sayah R, Lacoste V, Donadille Trompier F, Nauraye C, De Marzi L, Vabre I, Delacroix S, Hérault J and Clairand 2015 Monte Carlo modeling of proton therapy installations: a global experimental method to validate secondary neutron dose calculations *Phys Med Biol* **59** 2747–65

Fontenot J D, Newhauser W D and Titt U 2005 Design tools for proton therapy nozzles based on the double-scattering foil technique *Radiat Prot Dosim* **116** 211–5

Fontenot J D, Lee A K and Newhauser W D 2009 Risk of secondary malignant neoplasms from proton therapy and intensity-modulated x-ray therapy for early-stage prostate cancer *Int J Radiat Oncol Biol Phys* **74** 616–22

Fontenot J, Taddei P, Zheng Y, Mirkovic D, Jordan T and Newhauser W 2008 Equivalent dose and effective dose from stray radiation during passively scattered proton radiotherapy for prostate cancer *Phys Med Biol* **53** 1677–88

Geng C, Moteabbed M, Xie Y, Schuemann J, Yock T and Paganetti H 2015 Assessing the radiation-induced second cancer risk in proton therapy for pediatric brain tumors: the impact of employing a patient-specific aperture in pencil beam scanning *Phys Med Biol* **61** 12–22

Grahn D, Lombard L S and Carnes B A 1992 The comparative tumorigenic effects of fission neutrons and cobalt-60 gamma rays in the B6CF1 mouse *Radiat Res* **129** 19–36

Han S, Cho G and Lee S B 2017 An Assessment of the Secondary Neutron Dose in the Passive Scattering Proton Beam Facility of the National Cancer Center *Nucl Eng Technol* **49** 801–9

Hollander C F, Zurcher C and Broerse J J 2003 Tumorigenesis in high-dose total body irradiated rhesus monkeys--a life span study *Toxicol Pathol* **31** 209–13

Homann K, Howell R, Eley J, Mirkovic D, Etzel C, Giebeler A, Mahajan A, Zhang R and Newhauser W 2016 The need for individualized studies to compare radiogenic second cancer (RSC) risk in proton versus photon Hodgkin Lymphoma patient treatments *J Proton Ther* **1**

Hultqvist M and Gudowska I 2010 Secondary absorbed doses from light ion irradiation in anthropomorphic phantoms representing an adult male and a 10 year old child *Phys Med Biol* **55** 6633–53

ICRP 2003 Publication 92: Relative Biological Effectiveness (RBE), Quality Factor (*Q*), and Radiation Weighting Factor (w_R) *Ann ICRP* **33** (New York: Pergamon)

Jiang H, Wang B, Xu X G, Suit H D and Paganetti H 2005 Simulation of organ-specific patient effective dose due to secondary neutrons in proton radiation treatment *Phys Med Biol* **50** 4337–53

Kuhne W W, Gersey B B, Wilkins R, Wu H, Wender S A, George V and Dynan W S 2009 Biological effects of high-energy neutrons measured in vivo using a vertebrate model *Radiat Res* **172** 473–80

Matsumoto S, Koba Y, Kohno R, Lee C, Bolch W E and Kai M 2016 Secondary Neutron Doses to Pediatric Patients During Intracranial Proton Therapy: Monte Carlo Simulation of the Neutron Energy Spectrum and its Organ Doses *Health Phys* **110** 380–6

Moffitt G B, Stewart R D, Sandison G A, Goorley J T, Argento D C, Jevremovic T, Emery R, Wootton L S, Parvathaneni U and Laramore G E 2018 Dosimetric characteristics of the University of Washington Clinical Neutron Therapy System *Phys Med Biol* **63** 105008

Moyers M F, Benton E R, Ghebremedhin A and Coutrakon G 2008 Leakage and scatter radiation from a double scattering based proton beamline *Med Phys* **35** 128–44

Newhauser W D, Berrington de González A, Schulte R and Lee C 2016 A Review of radiotherapy-induced late effects research after advanced technology treatments *Front Oncol* **6** 13

Newhauser W D, Fontenot J D, Mahajan A, Kornguth D, Stovall M, Zheng Y, Taddei P J, Mirkovic D, Mohan R, Cox J D and Woo S 2009 The risk of developing a second cancer after receiving craniospinal proton irradiation *Phys Med Biol* **54** 2277–91

Newhauser W D, Schneider C, Wilson L, Shrestha S and Donahue W 2017 A review of analytical models of stray radiation exposures from photon- and proton-beam radiotherapies *Radiat Prot Dosim* **21**

Newhauser W D, Zheng Y, Taddei P J, Mirkovic D, Fontenot J D, Giebeler A, Zhang R, Titt U and Mohan R 2008 Monte Carlo proton radiation therapy planning calculations *T Am Nucl Soc* **99** 63–4

Pelowitz D B 2008 *MCNPX™ User's Manual* (Los Alamos, NM: Los Alamos National Laboratory)

Pérez-Andújar A, Newhauser W D and DeLuca P M 2009 Neutron production from beam-modifying devices in a modern double scattering proton therapy beam delivery system *Phys Med Biol* **54** 993–1008

Pérez-Andújar A, Newhauser W D, Taddei P J, Mahajan A and Howell R M 2013 The predicted relative risk of premature ovarian failure for three radiotherapy modalities in a girl receiving craniospinal irradiation *Phys Med Biol* **58** 3107–23

Pérez-Andújar A, Zhang R and Newhauser W 2013 Monte Carlo and analytical model predictions of leakage neutron exposures from passively scattered proton therapy *Med Phys* **40** 121714-1–11

Polf J C and Newhauser W D 2005 Calculations of neutron dose equivalent exposures from range-modulated proton therapy beams *Phys Med Biol* **50** 3859–73

Polf J C, Titt U and Newhauser W D 2005 Patient neutron dose equivalent exposures outside of the proton therapy treatment field *Radiat Prot Dosim* **115** 154–8

Rechner L A, Howell R M, Zhang R, Etzel C, Lee A K and Newhauser W D 2012 Risk of radiogenic second cancers following volumetric modulated arc therapy and proton arc therapy for prostate cancer *Phys Med Biol* **57** 7117–32

Schneider C, Newhauser W and Farah J 2015 An analytical model of leakage neutron equivalent dose for passively-scattered proton radiotherapy and validation with measurements *Cancers* **7** 795–810

Stokkevåg C H, Schneider U, Muren L P and Newhauser W 2017 Radiation-induced cancer risk predictions in proton and heavy ion radiotherapy *Phys Medica* **42** 259–62

Taddei P J, Fontenot J D, Zheng Y, Mirkovic D, Lee A K, Titt U and Newhauser W D 2008 Reducing stray radiation dose to patients receiving passively scattered proton radiotherapy for prostate cancer *Phys Med Biol* **53** 2131–47

Taddei P J, Khater N, Youssef B, Howell R M, Jalbout W T, Zhang R, Geara F B, Giebeler A, Mahajan A, Mirkovic D and Newhauser W D 2018 Low- and middle-income countries can reduce risks of subsequent neoplasms by referring pediatric craniospinal cases to centralized proton treatment centers *Biomed Phys Eng Express* **4** 025029

Taddei P J, Khater N, Zhang R, Geara F B, Mahajan A, Jalbout W, Pérez-Andújar A, Youssef B and Newhauser W D 2015 Inter-Institutional Comparison of Personalized Risk Assessments for Second Malignant Neoplasms for a 13-Year-Old Girl Receiving Proton versus Photon Craniospinal Irradiation *Cancers* **7** 407–26

Taddei P J, Mahajan A, Mirkovic D, Zhang R, Giebeler A, Kornguth D, Harvey M, Woo S and Newhauser W D 2010 Predicted risks of second malignant neoplasm incidence and mortality due to secondary neutrons in a girl and boy receiving proton craniospinal irradiation *Phys Med Biol* **55** 7067–80

Taddei P J, Mirkovic D, Fontenot J D, Giebeler A, Zheng Y, Kornguth D, Mohan R and Newhauser W D 2009a Stray radiation dose and second cancer risk for a pediatric patient receiving craniospinal irradiation with proton beams *Phys Med Biol* **54** 2259–75

Taddei P J, Mirkovic D, Fontenot J D, Giebeler A, Zheng Y, Titt U, Woo S and Newhauser W D 2009b Reducing stray radiation dose for a pediatric patient receiving proton craniospinal irradiation *Nucl Technol* **168** 108–12

Tayama R, Fujita Y, Tadokoro M, Fujimaki H, Sakae T, Terunuma T 2006 Measurement of neutron dose distribution for a passive scattering nozzle at the Proton Medical Research Center (PMRC) *Nucl Instrum Meth A* **564** 532–6

Wolf C, Lafuma J, Masse R, Morin M and Kellerer A M 2000 Neutron RBE for Induction of Tumors with High Lethality in Sprague-Dawley Rats *Radiat Res* **154** 412–20

Wroe A, Rosenfeld A and Schulte R 2007 Out-of-field dose equivalents delivered by proton therapy of prostate cancer *Med Phys* **34** 3449–56

Zacharatou Jarlskog C, Lee C, Bolch W E, Xu X G and Paganetti H 2008 Assessment of organ specific neutron equivalent doses in proton therapy using computational whole-body age-dependent voxel phantoms *Phys Med Biol* **53** 693–717

Zhang R, Howell R M, Giebeler A, Taddei P J, Mahajan A and Newhauser W D 2013 Comparison of risk of radiogenic second cancer following photon and proton craniospinal irradiation for a pediatric medulloblastoma patient *Phys Med Biol* **58** 807–23

Zhang R, Howell R M, Taddei P J, Giebeler A, Mahajan A and Newhauser W D 2014 A comparative study on the risks of radiogenic second cancers and cardiac mortality in a set of pediatric medulloblastoma patients treated with photon or proton craniospinal irradiation *Radiother Oncol* **113** 84–8

Zhang R, Pérez-Andújar A, Fontenot J D, Taddei P J and Newhauser W D 2010 An analytic model of neutron ambient dose equivalent and equivalent dose for proton radiotherapy *Phys Med Biol* **55** 6975–85

Zheng Y, Fontenot J, Taddei P, Mirkovic D and Newhauser W 2008 Monte Carlo simulations of neutron spectral fluence, radiation weighting factor and ambient dose equivalent for a passively scattered proton therapy unit *Phys Med Biol* **53** 187–201

Zheng Y, Newhauser W, Fontenot J, Koch N and Mohan R 2007a Monte Carlo simulations of stray neutron radiation exposures in proton therapy *J Nucl Mater* **361** 289–97

Zheng Y, Newhauser W, Fontenot J, Taddei P and Mohan R 2007b Monte Carlo study of neutron dose equivalent during passive scattering proton therapy *Phys Med Biol* **52** 4481–96

Table 1. Treatment parameters for the intracranial proton boost fields of the girl and boy in this study and the previous MC studies (Taddei *et al* 2009a, Taddei *et al* 2010). Abbreviations: left posterior oblique (LPO), posterior-anterior (PA), right posterior oblique (RPO), and left lateral (LL).

	Girl			Boy	
Beam	1	2	3	1	2
Beam orientation	LPO	PA	RPO	LPO	LL
Gantry angle (degree)	97	180	263	130	90
Nominal beam energy (MeV)	160	180	160	160	140
Maximum range in patient (cm H_2O)	12.0	13.5	12.0	11.3	9.2
SOBP width (cm)	8.0	8.0	8.0	7.0	6.0
Collimated field, major axis (cm)	6.6	7.0	6.3	11.8	11.6
Collimated field, minor axis (cm)	6.3	6.3	6.3	5.5	5.4
Air gap (cm)	23.0	29.0	23.0	2.0	2.0
Aperture thickness (cm)	4	6	4	4	4

Table 2. Adjustment factors used to translate the LSU-MDA model for use with clinical beams. F_{wR}, F_{SOBP}, F_{as}, and F_g were the adjustment factors for radiation weighting factor (w_R), spread-out Bragg peak, aperture size, and air gap, respectively. Because F_{wR} varied for each voxel, the average is reported. Additionally, mean w_R values for the fields of the girl and boy from the previous MC studies are listed (Taddei *et al* 2009a, Taddei *et al* 2010).

	Girl			Boy	
Beam	1	2	3	1	2
F_{as}	0.930	0.930	0.930	0.900	0.890
F_{SOBP}	1.800	1.800	1.800	1.750	1.690
F_g	0.680	0.550	0.680	2.220	2.220
F_{wR}	1.710	1.750	1.710	1.730	1.700
mean w_R of MC studies	9.410	9.410	9.430	9.540	9.730

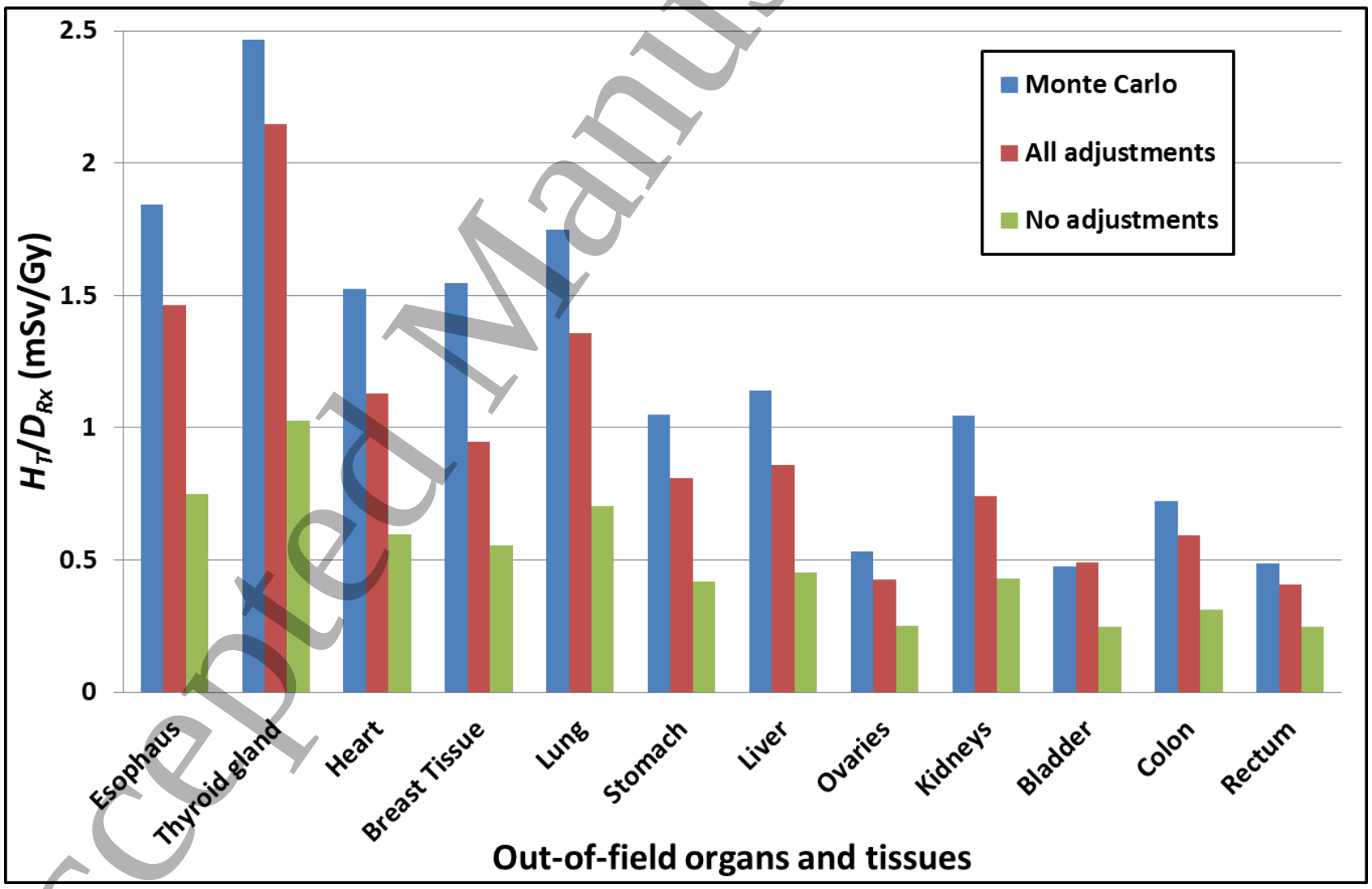

Figure 1. H_T/D_{Rx} from external neutrons for the composite of the intracranial boost fields of the girl. The mean organ doses were estimated by MC simulations (blue), the model with all adjustments (red), the model with no adjustments (green).

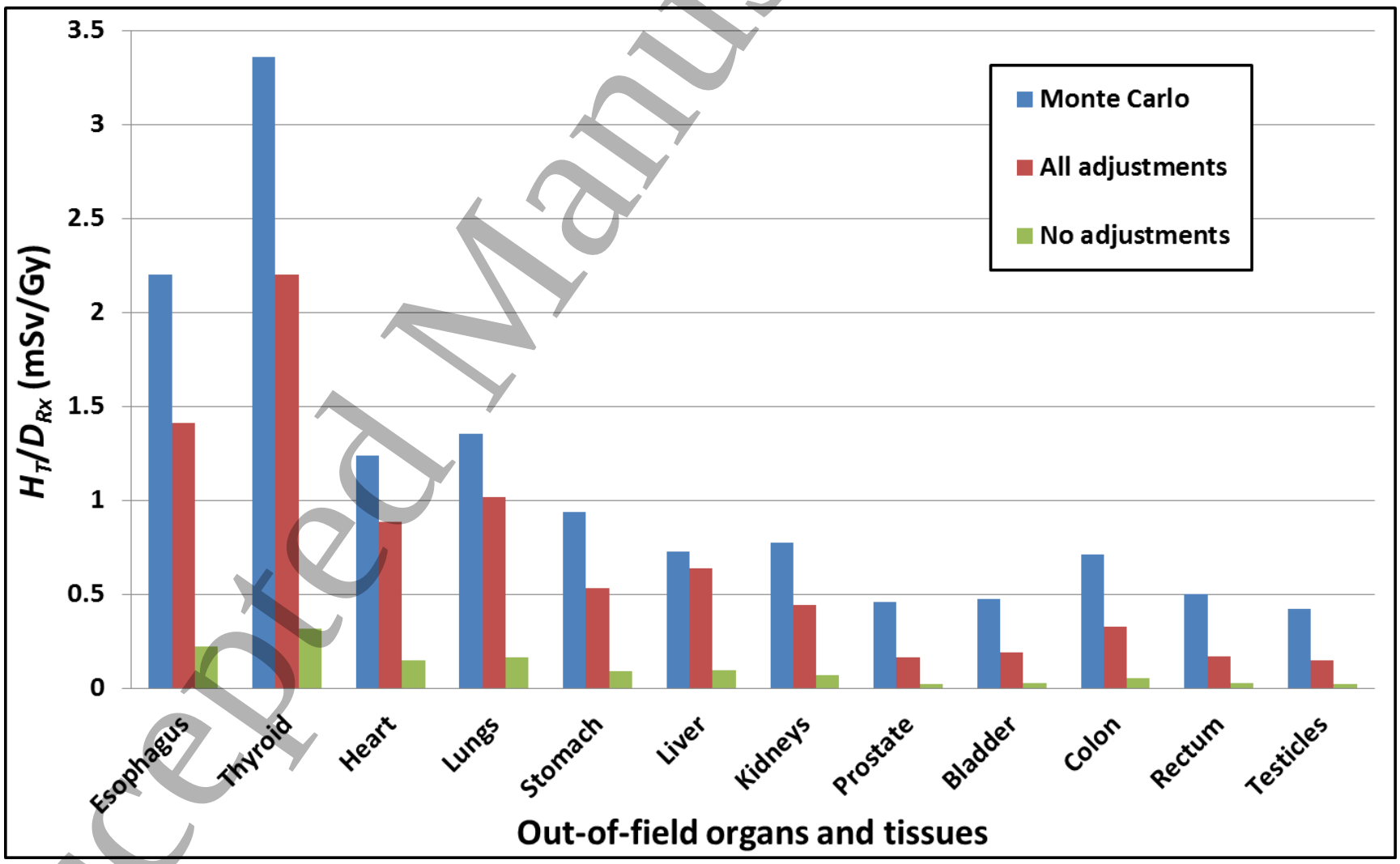

Figure 2. H_T/D_{Rx} from external neutrons for the composite of the intracranial boost fields of the boy. The mean organ doses were estimated by MC simulations (blue), the model with all adjustments (red), the model with no adjustments (green).